ACS Catalysis

Research Article

pubs.acs.org/acscatalysis

Shape and Transition State Selective Hydrogenations Using Egg-Shell Pt-MIL-101(Cr) Catalyst

Hossein Khajavi,*[,†] Hans A. Stil,[‡] Herman P. C. E. Kuipers,[‡] Jorge Gascon,*[,†] and Freek Kapteijn[†]

[†]Catalysis Engineering, Chemical Engineering Department, Delft University of Technology, Julianalaan 136, 2628 BL Delft, The Netherlands

[‡]Shell Global Solutions, Projects and Technology, Innovation & Research/Team Experimentation (PTI/TX), Shell Technology Center Amsterdam, Grasweg 31, 1031 HW, Amsterdam, The Netherlands

Supporting Information

ABSTRACT: The use of the metal organic framework MIL-101(Cr) as support for Pt nanoparticles is evaluated in three selective hydrogenation reactions. Homogenous Pt nanoparticles of ∼4 nm can be formed inside the porosity of MIL-101(Cr) in close contact with the Cr trimers in an egg-shell configuration by a wet impregnation procedure combined with sonication. The catalyst is applied in the selective hydrogenations of olefin mixtures, benzonitrile, and linoleic acid. In the case of an olefin mixture, 1-octene is selectively hydrogenated over 1-hexadecene, attributed to diffusion limitations that favor the hydrogenation of the smaller substrate. In the case of benzonitrile hydrogenation, benzylamine is selectively formed over dibenzylamine attributed to transition state selectivity. In the hydrogenation of linoleic acid, selectivities were similar to that for platinum on alumina.

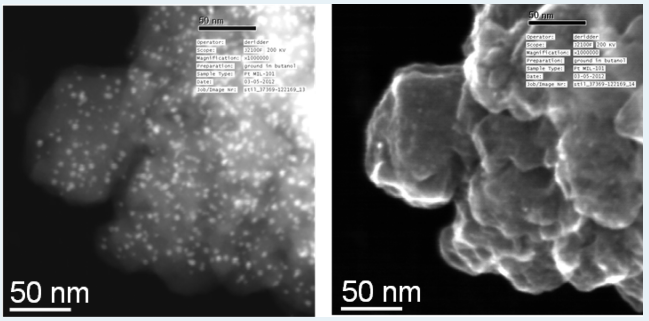

KEYWORDS: *metal organic frameworks, MIL-101, catalysis, platinum nanoparticles, selective hydrogenation, benzonitrile*

1. INTRODUCTION

Metal organic frameworks (MOFs) have become a familiar term in the world of ordered porous solids. With nearly two decades of research into this category of materials, we are now seeing a wide range of potential applications being assessed at both academic and industrial levels. These potential applications range from (size/shape selective-) catalysis[1−11] and adsorption/separation processes[12−17] to advanced applications such as semiconductors,[18−25] photoluminescence,[26−31] and drug delivery.[32−34] The lattice structure of a MOF consists of inorganic nodes that are bridged by multidentate organic linkers, often resulting in highly porous crystals with a high degree of tunability. By virtue of the vast amount of possible combinations of organics and inorganics, a countless number of structures are conceivable; this is reflected in the nearly 25 000 structures that have been identified to date,[34] many of them exhibiting unprecedented pore volumes.

When it comes to catalytic applications, several routes can be followed, with the MOF acting as the active catalyst or as the support for the species of interest. The immobilization of homogeneous catalysts on MOFs to heterogeneous catalysts is of high interest and has been pursued because of the intrinsic advantages heterogeneous catalysts have.[9] The coupling of shape selectivity and catalysis has also been demonstrated using MOFs[3] alongside catalysis by the inorganic nodes,[7] incorporated catalytically active metals,[1,5,7−9,35] (metal-) organics,[4,36,37] postsynthetically functionalized linkers,[37] and the combination of several functionalities in one single MOF catalyst.[38]

The use of MOFs as nanomolds for hosting functional inorganic nanoparticles and their application in catalysis and hydrogen storage has attracted increasing attention during the past few years.[39] Depending upon the method and the conditions applied for the loading and transformation of precursors, nanoparticle encapsulation might be only partially successful. Three possible case scenarios have been defined when classifying metal nanoparticle distributions in MOFs:[39] (i) in class A, most of the nanoparticles are preferentially deposited at the outer surface of a MOF crystal, resulting in a wide particle size distribution and a poor metal dispersion, especially in the case of high loadings; (ii) in class B, most of the nanoparticles are deposited in the pore space of the MOF, but they display a rather broad particle size distribution that might arise from partial destruction of the MOF skeleton during impregnation; and (iii) in class C, nanoparticles with a homogeneous particle size distribution close to that of the MOF pores or cavities are evenly distributed throughout the porosity of the host.[5,7,8,10,37−47] A critical evaluation of most presented results demonstrates that MOF-encapsulated metal nanoparticles do not display outstanding activity. The relatively

Received: August 14, 2013
Revised: September 23, 2013
Published: October 2, 2013

low activity should not be surprising, since in most cases, catalytic reactions in which the use of a MOF as support does not present any advantage (e.g., structure insensitive reactions) and may even add undesired diffusion limitations have been explored. In contrast, for catalytic applications in which control of nanoparticle size and morphology is needed, or in which well-defined pores may favor shape-selective conversions or certain transition states, MOFs may offer unique advantages over other nanostructured supports, as demonstrated in this work.

In this paper, the introduction of platinum nanoparticles in MIL-101(Cr) is reported. A high dispersion is achieved and the application of the resulting catalyst in the hydrogenation of 1-octene, 1-hexadecene, benzonitrile, and linoleic acid is demonstrated. The selected reactions are intended to demonstrate both substrate and product selectivity. These reactions are well understood in terms of mechanisms and kinetics, so highly suited for this type of study. The simultaneous hydrogenation of two linear α-olefins, 1-octene and 1-hexadecene, with a significant difference in chain length, demonstrates how mass transport limitations can favor substrate selectivity (shape selectivity) in MOFs. In the hydrogenation of benzonitrile, restrictive transition state selectivity is demonstrated, whereby the formation of side products is suppressed. Linoleic acid hydrogenation occurs similarly to that of over a conventional Pt catalyst.

2. EXPERIMENTAL SECTION

2.1. Materials. All chemicals, unless explicitly specified, were purchased from Sigma−Aldrich and were used without any further purification: terephthalic acid (97%), chromium(III) nitrate nonahydrate (99%), hexachloroplatinic acid (37.4 wt % Pt basis), hydrofluoric acid (47−51 wt %), ethanol (99.8%), tetrahydrofuran anhydrous and inhibitor free (≥99.9%), formaldehyde solution (36.5−38% aqueous), 1-octene (98%), 1-hexadecene (≥99%), benzonitrile anhydrous (≥99%), linoleic acid (>99.0%) and *N*-methyl-*N*-(trimethylsilyl)trifluoroacetamide (MSTFA, suitable for silylation). A 1 wt % platinum on alumina catalyst (Sigma−Aldrich) was used as a reference in the catalytic performance testing.

2.2. Catalyst Preparation. For the synthesis of MIL-101(Cr), a microwave procedure was optimized. A solution composed of chromium(III) nitrate nonahydrate (9.765 g, 24.5 mmol), terephthalic acid (3.652 g, 22.0 mmol), hydrofluoric acid (0.90 g, ≈22 mmol), and water (90.0 mL) was heated using a MycroSYNTH Plus ACT38. A program was applied that ramped the temperature from ambient to 483 K within 5 min; subsequently, this temperature was maintained for 45 min. The microwave oven was operated at 600 W, with a 50 rpm autoclave rotation and 120 rpm stirring rate for the magnetic stirrer inside of the autoclave reactor. After this, the autoclave was allowed to cool and settle overnight without agitation, stirring, or opening. The resulting product is vacuum-filtered using a 0.1 μm regenerated cellulose filter and washed with ethanol under reflux overnight. A second washing step is applied with tetrahydrofuran in a Soxhlet for at least 24 h. Finally, the sample is filtered off and dried at 423 K for a minimum of 12 h under a mild vacuum (≈100 mbar) to produce "MIL-101(Cr) *as prepared*".

For the platinum impregnation, 0.657 g of the prepared MIL-101 was suspended in 10 mL of ethanol. A second solution containing 40 mg (0.10 mmol) of hexachloroplatinic acid in 5 mL of water is prepared. The hexachloroplatinic acid solution is added dropwise to the MIL-101 slurry and stirred at room temperature for several hours before adding 0.44 mL of aqueous formaldehyde. The resulting slurry is then ultrasonicated in a sealed round-bottom flask overnight at 308 K. This treatment is continued for an additional 24 h with the round-bottom flask open in a fume hood and, after that, at 343 K until the majority of the solvent has evaporated. While still warm, the inside of the round-bottom flask is scratched and left to cool so as to crystallize unadsorbed platinum onto the flask walls. The resulting material is recovered by filtration and washed with tetrahydrofuran in a Soxhlet overnight and dried in air in multiple stages at temperatures of 323, 343, and 373 K, with each temperature being maintained for a minimum of 5 h ("MIL-101(Cr) *Pt partially reduced*"). An additional reduction step using a flow of 15 mL min^{-1} of 2% diluted hydrogen at 373 K results in "MIL-101(Cr) Pt *fully reduced*" (also referred to as "Pt-MIL-101(Cr) catalyst"). An additional sample has been prepared by omitting the reducing steps; "MIL-101(Cr) *Pt loaded*".

2.3. Characterization. After a pretreatment at 443 K under vacuum (10^{-4} mbar) overnight, N_2 adsorption at 77 K (Quantachrome Autosorb-6B) was used to determine the specific BET surface area (calculated from data between 0.05 and 0.2 relative pressures). Pore volume was calculated at 0.5 relative pressure. For elemental analysis, samples were digested in a mixture of 1% hydrofluoric acid and 1.25% sulfuric acid and analyzed with an ICP-OES Perkin-Elmer Optima 3000 dv for platinum and chromium. Active phase loss has been studied by the analysis of the tested reaction mixtures for Pt after filtering of the Pt-MIL-101(Cr) catalyst. The crystalline structure of the catalyst composite has been analyzed using a Bruker-AXS D5005 theta/theta diffractometer equipped with incident beam Cu Kα1 monochromator. The range of 1−20 2θ (°) has been scanned for a period of 90 min. Unless stated explicitly, all scans were done under ambient conditions.

Using FT-IR analysis of CO adsorption at low temperature, Brønsted and Lewis acid sites in the samples were distinguished. For this, samples were prepared by pressing the MOF or MOF composite powder and KBr at 1 ton·in.$^{-2}$. The pellets were pretreated under high vacuum at 423 K initially to remove adsorbed species. After this, the samples were reduced in situ in a flow of 15 mL min^{-1} of 2% diluted hydrogen at 373 K, which was followed by a repeat of the pretreatment step. Subsequently, the samples were cooled to 143 K, still under vacuum, and CO was dosed to 5 mbar. After this, the sample was brought to room temperature, and helium was charged into the sample holder, equipped with two CaF_2 windows. Using a Thermo Nicolet Nexus 6700 and iS50R FT-IR spectrometer, diffuse reflectance infrared Fourier transformed (DRIFT) spectra were recorded. These spectrometers are equipped with a DRIFT cell with conical pellet holders, KBr beam splitter, DTGS-TEC detector (range 11 000−375 cm^{-1}; Nicolet 6700), liquid-nitrogen-cooled MCT-B detector (range 11 000−400 cm^{-1}; Nicolet iS50R), and a 633-nm monochromatic laser beam. The spectra were recorded from 4000 to 400 cm^{-1} after an accumulation of a minimum of 64 scans and a resolution of 4 cm^{-1}. KBr was used to perform all background measurements. CO chemisorption experiments were done in the same setup at room temperature.

XPS spectra were recorded on an AXIS Ultra HSA spectrometer (operating pressure <10^{-9} mbar) with a 165 mm radius hemi-spherical analyzer (HSA) in rapid unscanned mode using a delay-line detector (DLD). This was done to

dx.doi.org/10.1021/cs400681s | *ACS Catal.* 2013, 3, 2617−2626

reduce potential damage due to sample irradiation, which was observed during scanned mode. Spectra obtained used an aluminum anode (Al Kα = 1486.6 eV). The coaxial charge neutralizer ensures uniform charge compensation over the sample, despite inhomogeneity. Samples were deposited on a sample holder using double-sided adhesive and subsequently evacuated under high vacuum. After degassing, samples were transferred to the analysis chamber. Region scans were measured at 40 eV, and survey scans, at a constant pass energy of 160 eV, all at room temperature. Calibration of binding energies was referenced to the C *1s* line at 284.6 eV from adventitious carbon. Surface atomic ratios have approximated using the integrated intensities of peaks corrected by the atomic sensitivity factors.[48]

High-resolution (scanning-)transmission electron microscopy (STEM) was performed on a JEOL 2100F equipped with a Gatan Erlangshen ES500W, an Orius SC1000 CCDs, a Gatan Tridiem energy filter system, and a Gatan 806 high-angle annular dark-field (HAADF) STEM detector. The microscope was operated at an accelerating voltage of 200 kV (FEG, range 80−200 kV), with a 0.17 nm point resolution. For the STEM analysis, a 0.7 nm of probe size, 40 μm of condensor aperture, and 7 cm of camera length of HAADF detector were used. HAADF and secondary electron imaging (SEI-Components) images were taken with a nominal spot size of 0.5 nm. Energy dispersive X-ray (EDX) spectrum profile scanning was performed using the STEM attachment. For all techniques, low-intensity beam conditions were applied to minimize the electron dose and beam damage to the sample (using the maximum possible magnification, minimal beam intensity, and long exposure durations).

2.4. Catalytic Performance Testing. The selective hydrogenation of 1-octene and 1-hexadecene was carried out in semibatch mode at a constant pressure of 1.5 bar absolute of hydrogen, at 308 K and at a concentration of 40.5 mmol 1-octene/mg Pt and 40.5 mmol 1-hexadecene/mg Pt. Here, the reaction selectivity ratio is quantified and is defined as the ratio of converted 1-octene to converted 1-hexadecene.

The selective hydrogenation of pure benzonitrile was carried out at 36.5 mmol benzonitrile/mg Pt at 20 bar and 308 K. Primary (aromatic) amines are important chemicals and pharmaceutical intermediates and are also in solvents, paints, herbicides, and used in the textile industry. They are produced by heterogeneously catalyzed hydrogenation of aromatic nitriles.[49−54] The hydrogenation of benzonitrile often yields various products; namely, benzylamine (primary amine), dibenzylamine (secondary amine), *N*-benzylidenebenzylamine (ternary amine), benzylideneimine, α-aminodialkylamine, and toluene.[55] Reaction Scheme 1 presents the possible pathways.[52−59]

The hydrogenation of linoleic acid and its product oleic acid is the third reaction investigated. The reaction was carried out using a reagent-to-catalyst ratio of 26 mmol linoleic acid/mg Pt, under 20 bar of hydrogen atmosphere at 308 K. Scheme 2 illustrates simplified reaction pathways of hydrogenation and isomerization of linoleic acid using a heterogeneous catalyst.[60−67]

The initial rate of consumption of reagents is presented as a turnover frequency (*TOF*), defined here as

$$TOF = \frac{r \cdot N_{\text{Avogadro}}}{A_{\text{Pt}} \cdot \rho_{\text{sites}}}$$

Scheme 1. Possible Reaction Pathways in the Hydrogenation of Benzonitrile (BN)[a]

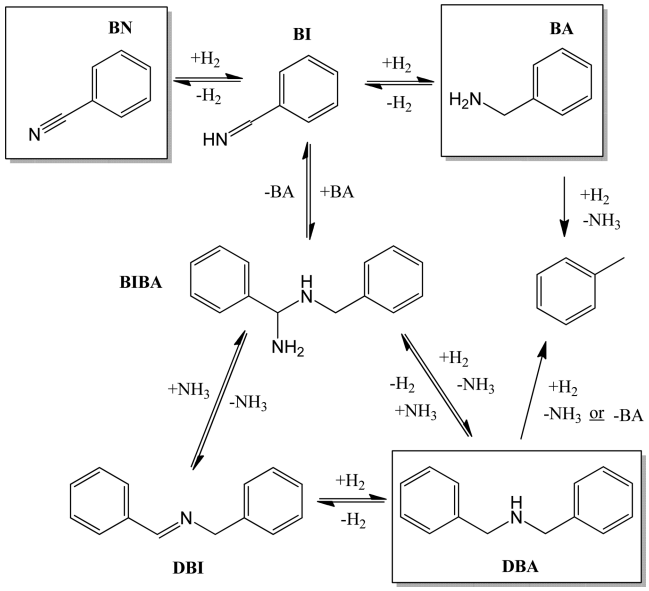

[a]The hydrogenation of BN results in the formation of benzylamine (BA) through the intermediate benzylideneimine (BI). Condensation of BA and BI occurs through the intermediate α-aminodialkylamine (BIBA) and *N*-benzylidenebenzylamine (DBI) to dibenzylamine (DBA). Hydrogenolysis yields toluene from DBA and BA. The direct hydrogenolysis of BIBA to DBA is also possible. The reagent and main products have been boxed.

Scheme 2. A Simplified Scheme of Possible Reaction Pathways to the Various Products Formed in the Hydrogenation and Isomerization of Linoleic Acid (Boxed) As Typically Described in Literature for Noble Metal Heterogeneous Catalysts[61,a]

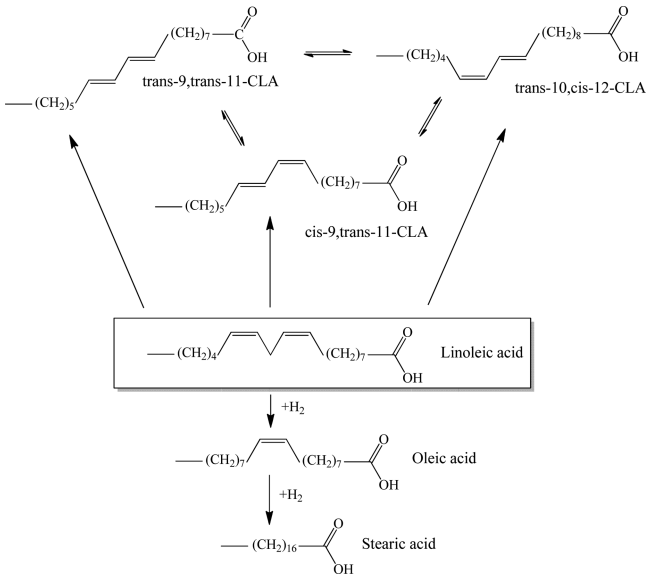

[a] Products such as elaidic acid and *cis*-/*trans*-vaccenic acid have not been included in this schematic.

The ratio of the reaction rate (r, with units of mol g_{Pt}^{-1} s^{-1}) multiplied by Avogadro's constant (N_{Avogadro}; mol^{-1}) to the specific surface area of platinum (A_{Pt}, with units of m^2 g^{-1})

dx.doi.org/10.1021/cs400681s | ACS Catal. 2013, 3, 2617−2626

multiplied by active site density per Pt surface area (ρ_{sites}, with units of sites m^{-2}). The reaction rate is defined here as

$$r = \frac{dC_{reagent}}{dt} \cdot \frac{1}{C_{Pt}}$$

Thus, the reaction rate is given by the initial rate of reagent consumption divided by the mass concentration of platinum per reagent volume (C_{Pt}, with units of g m^{-3}). Reagent conversion (X) is defined as a ratio of the consumed reagent ($C_0 - C$) to the initial concentration (C_0):

$$X = \frac{C_0 - C}{C_0}$$

3. RESULTS

3.1. Textural Characterization. The use of microwave synthesis for MIL-101(Cr)[68] results in very homogeneous MOF crystals, making separation of the MOF phase from unreacted terephthalates[69,70] straightforward. The optimized procedure for the impregnation of the metal precursor involved the use of water−ethanol mixtures in combination with ultrasonication. The latter was found crucial: without the use of ultrasonication during the wet impregnation step, the majority of platinum was deposited on the outer surface of MIL-101(Cr) crystals (Supporting Information Figure S6a).

X-ray diffraction patterns of the unmodified MIL-101(Cr) (MIL-101(Cr) *as prepared*), partially reduced hexachloroplatinic acid impregnated MIL-101 ("MIL-101(Cr) *Pt partially reduced*"), platinum impregnated MIL-101 catalyst ("MIL-101(Cr) *Pt fully reduced*"), and the used platinum impregnated MIL-101 catalyst ("MIL-101(Cr) *used catalyst*") are illustrated in Figure 1. Here, partial reduction refers to reduction by formaldehyde, and complete reduction refers to the use of an additional step with a hydrogen gas stream at 373 K (for the full diffraction pattern, please refer to the Supporting Information; S1). The collected diffraction patterns match that of the simulated extended MTN topology of MIL-101(Cr) found in the literature[69−71] in all cases. The crystallinity of the produced samples is affected by the hexachloroplatinic acid impregnation, although this change is subtle. It can also be deduced that the used catalyst maintains its phase structure even after extensive usage. The diffraction peak height ratios are the same in all samples; however, after the wet impregnation step, samples have less clearly defined peaks, but peak intensities are unaffected.

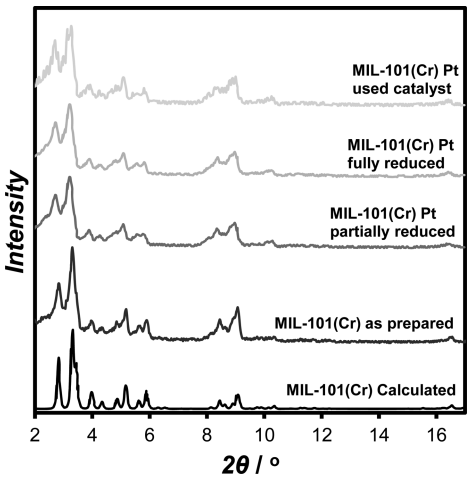

Figure 1. X-ray diffraction patterns of MIL-101(Cr) calculated,[67−69] the unmodified MIL-101(Cr) (MIL-101(Cr) *as prepared*), partially reduced hexachloroplatinic acid impregnated MIL-101 (MIL-101(Cr), *Pt partially reduced*), platinum impregnated MIL-101 as the prepared catalyst (MIL-101(Cr) *Pt fully reduced*), and the used platinum impregnated MIL-101 catalyst after 180 h for the hydrogenation of linoleic acid (MIL-101(Cr) *used catalyst*).

The nitrogen adsorption isotherms for MIL-101(Cr) *as prepared* and MIL-101(Cr) *Pt fully reduced*, before and after catalytic testing, shown in Figure 2, all correspond well to previously reported isotherms for MIL-101(Cr). At low relative pressures (P/P_0 = 0.2), two steps that are attributed to the filling of the two different cavities in MIL-101 are observed. At relative pressures below 0.05, the supertetrahedra of MIL-101 are filled, with increasing pressure; the medium cavities start being filled at P/P_0 = 0.1, and the larger cavities are filled at relative pressures of 0.2.

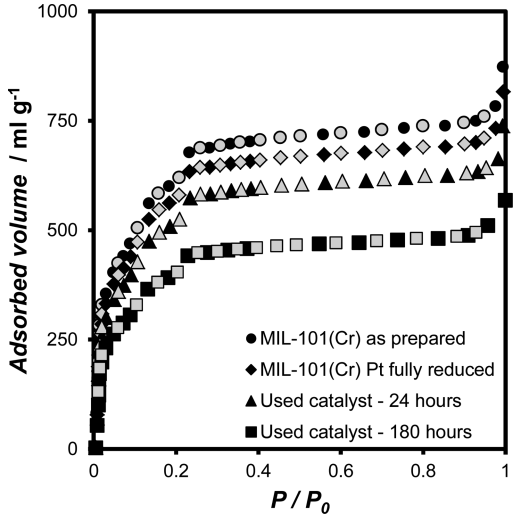

Figure 2. Nitrogen adsorption isotherms for MIL-101(Cr) *as prepared*, fresh platinum impregnated MIL-101 catalyst (MIL-101(Cr) *Pt fully reduced*), and used platinum impregnated MIL-101 catalyst after 24 and 180 h for the hydrogenation of linoleic acid. Solid black data points represent adsorption, and gray data points represent desorption.

The apparent BET surface areas are listed in Table 1 along with ICP Pt/Cr and XPS Pt/Cr atomic ratio analysis. Loadings of 1 wt % of Pt hardly result in any surface area loss. In contrast,

Table 1. Calculated BET Surface Areas, Atomic Ratio Pt/Cr Calculated from XPS Data and the Pt/Cr Atomic Ratio Obtained from ICP for Unmodified MIL-101 (MIL-101 *as prepared*), Platinum Impregnated MIL-101 catalyst (MIL-101(Cr) *Pt fully reduced*), and Used Platinum Impregnated MIL-101 Catalyst after 24 and 180 h for the Hydrogenation of Linoleic Acid (used catalyst, 24 and 180 h)

	N_2 adsorption	ICP	XPS
	BET surface area (m^2 g^{-1})	Pt/Cr	Pt/Cr
MIL-101(Cr) as prepared	2210		
MIL-101(Cr) Pt fully reduced	2180	0.12	0.261
Used catalyst 24 h	2120	0.11	
Used catalyst 180 h	1680	0.09	

dx.doi.org/10.1021/cs400681s | *ACS Catal.* 2013, 3, 2617−2626

a considerable loss is observed for the used catalyst, and this loss increases with the catalyst usage. After 180 h of use, the 1.2 wt % platinum impregnated MIL-101 loses ~23% of its surface area. This area loss was most noticeable in the case of linoleic acid hydrogenation. In other cases, the largest area loss was <11% for the hydrogenation of pure hexadecene (solvent-free) after 100 h. The spent catalyst could be reactivated by means of an overnight heat treatment at 443 K under hydrogen atmosphere. This resulted in the elimination of weakly adsorbed hydrocarbons, as followed from the TGA analysis (for TGA before and after reactivation, please refer to the Supporting Information; S2).

3.2. FT-IR Spectroscopy. Figure 3 illustrates the measured spectra in the region of interest (2060−2220 cm^{-1}) for a single

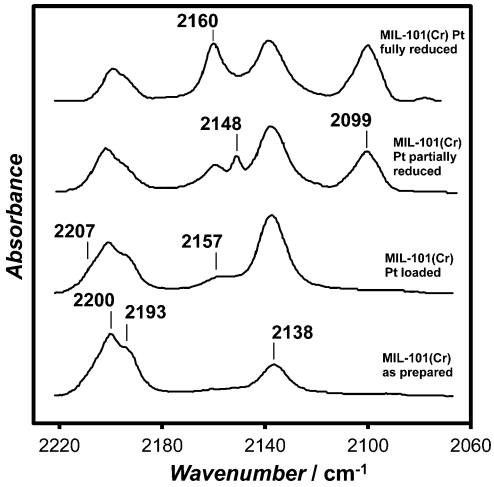

Figure 3. In situ FT-IR spectra of CO adsorption at 143 K on MIL-101(Cr) *as prepared*, MIL-101(Cr) *Pt loaded*, MIL-101(Cr) *Pt partially reduced*, and MIL-101(Cr) *Pt fully reduced* are measured.

batch of prepared sample after various treatments. In Figure 3; MIL-101(Cr) *Pt loaded* refers to hexachloroplatinic acid adsorbed by MIL-101(Cr). This is done by removing the formaldehyde reducing agent from the wet impregnation procedure. The band observed at 2099 cm^{-1} is associated with Pt^0−CO species[72−76] and is visible only in samples that contain the reduced hexachloroplatinic acid. The physisorption of CO is observed at 2138 cm^{-1}.[77] Bands observed at 2148 cm^{-1} are assigned to cationic platinum species and are a strong indicator for the formation of Pt^{2+}−CO upon CO dosing.[72−76] It is interesting that $\nu(Pt^{2+}-CO)$ bands are clearly observed only in the partially reduced platinum loaded sample, and almost not at all in the hexachloroplatinic acid-loaded MIL-101(Cr). We associate this phenomenon with the fact that Cl^- ligands are removed upon treatment with H_2 at moderate temperatures, allowing coordination of CO.

The band centered at 2160 cm^{-1} corresponds to CO interacting with Brønsted acid species found in the samples (75). This band is red-shifted to 2157 cm^{-1} in samples in which hexachloroplatinic acid is present. The OH groups identified could arise from strongly bound ethanol molecules that remain in the sample after the wet impregnation step, despite vacuum treatments. It is highly unlikely that these are terminal OH groups found from PtO formed on the surface of Pt nanoparticles because these are generally observed at 3497 and 3544 cm^{-1}.[78] Because of the inert atmosphere measured samples have been exposed to and the pretreatment of samples prior to measurements, such bands at 3497 and 3544 cm^{-1} have not been observed.

In Figure 3, the three characteristic ν(CO) bands can be observed at 2193, 2200, and 2207 cm^{-1} to various degrees in all measured samples attributed to the presence of open Cr^{3+} sites. The heterogeneous nature of Cr^{3+} sites is ascribed to the presence of fluoride ions on the chromium trimers[77] (HF being the source of fluoride ions during MOF synthesis). These bands are assigned to CO coordinated at Lewis acid sites. By increasing the reduced platinum content in the sample, the bands at 2193 and 2207 cm^{-1} become less distinct; this has been associated with the formation of platinum nanoparticles in close proximity of chromium trimers. The area of these bands also decreased as the Pt^0 became the dominant form of platinum present in the sample. The average size of the Pt nanoparticles in the fresh catalyst has been determined by CO chemisorption to be 4.3 nm, corresponding to a dispersion of 27%,[70−81] assuming a CO/Pt ratio of unity. This calculated size of the platinum nanoparticles exceeds the size of a single MIL-101 cage.

3.3. X-ray Photoelectron Spectroscopy. The surface composition of partially and fully reduced platinum-loaded MIL-101 catalyst has been analyzed by XPS. The complete spectral survey showing Pt *4f*, C *1s*, N *1s*, O *1s*, and Cr *2p* is shown in Figure 4, including the deconvolution of the Pt *4f*

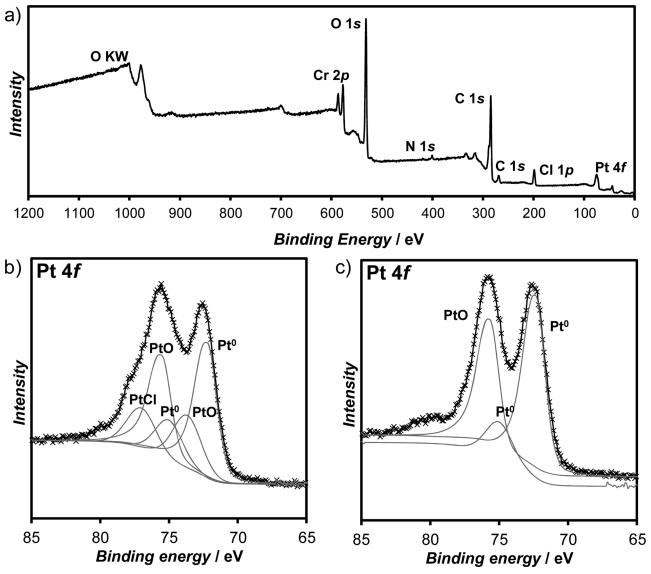

Figure 4. (a) XPS survey spectrum of the MIL-101(Cr) *Pt partially reduced* catalyst and the deconvolution of Pt *4f* region (70−80 eV) showing the various platinum oxidation states for (b) the MIL-101(Cr) *Pt partially reduced* and (c) the MIL-101(Cr) *Pt fully reduced*.

range. Three different platinum species can be found: namely, Pt^0 (72.20 and 75.53 eV), PtO (73.70 and 77.03 eV), and PtCl (80.28 eV). The formation of PtO is due to the exposure of the sample to ambient air atmosphere (70−74), and the presence of PtCl indicates that the sample has not been fully reduced under the experimental conditions (MIL-101(Cr) *Pt partially reduced*). Using the sensitivity factors, the atomic percentages of Cl to platinum has been calculated to be less than 0.01. Typical binding energy values have been observed for C *1s* at 284.5 (C−C/C−H), 285.66 (C−O), 288.52 (O−C═O), and 290.76 (C═O) eV. The N *1s* and O *1s* peaks have also been observed, although little information can be taken from these peaks. The

dx.doi.org/10.1021/cs400681s | ACS Catal. 2013, 3, 2617−2626

binding energy values observed for Cr *2p* are 577.19 and 586.78 eV. Both correspond to typical binding energies for Cr^{3+}. Other oxidation states of chromium are not observed, so the chromium trimers are not chemically modified by the platinum precursor during impregnation or during the reducing steps. The fully reduced sample (MIL-101(Cr) *Pt fully reduced*) shows a binding energy of 75.53 eV for the Pt $4f_{7/2}$ and 72.20 eV for the $4f_{5/2}$.

3.4. Scanning-Transmission Electron Microscopy (STEM). Figure 5 shows a STEM micrograph obtained from

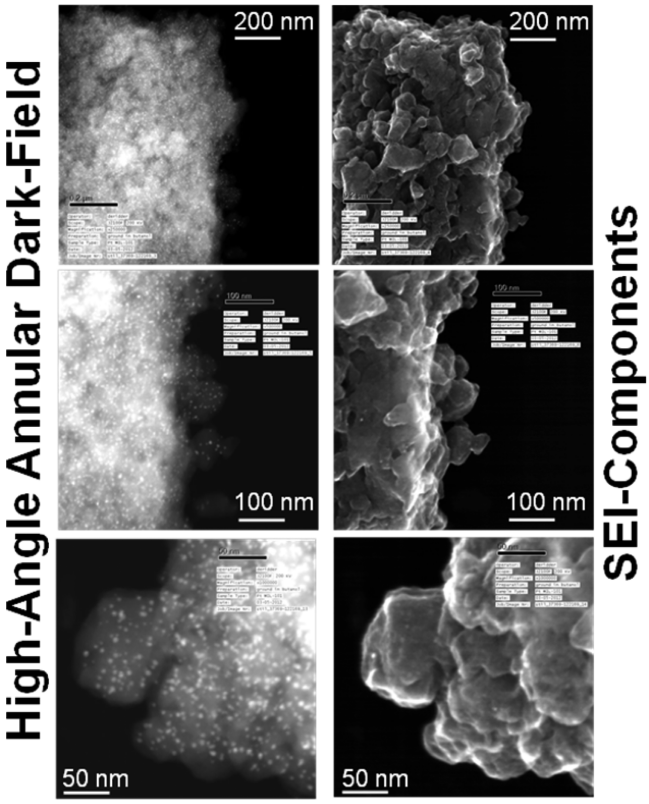

Figure 5. (S)TEM images showing HAADF (left) and SEI-components (right) of 1.2 wt % MIL-101(Cr) *Pt fully reduced* catalyst at various magnifications.

a 1.2 wt % platinum MIL-101(Cr) *Pt fully reduced* catalyst. The platinum nanoparticles are all dispersed throughout the sample with mean diameters of 5 ± 0.5 nm, which are in agreement with the values found by FTIR transmission spectroscopy combined with CO adsorption. The platinum nanoparticles are almost exclusively found inside the MIL-101 crystal and mostly in the outer region. By the comparison of ICP and XPS results, the bulk distribution of Pt across the framework can be deduced. Comparison between the measured Pt/Cr atomic ratio in the bulk (0.12), with XPS (Pt/Cr = 0.261), widely accepted as a surface analysis-based technique, indicates that the vast majority of platinum in the (inner) cages is close to the outer surface of the MIL-101 crystals, in an egg-shell configuration. In addition, the comparison of SEI components, a technique applied here to show platinum nanoparticles (white spots) at the external surface of the MIL-101 crystal, with the HAADF images that show all platinum nanoparticles in the crystal, evidence the scarcity of platinum nanoparticles at the outer surface of the crystals. In-depth analysis using energy dispersive X-ray analysis (EDX) confirms that platinum nanoparticles are being imaged.

3.5. Catalytic Performance Testing. The unmodified MIL-101(Cr) was inactive for all test reactions under the selected conditions. In the case of olefin hydrogenation, platinum on alumina demonstrated hardly any selectivity for octene over hexadecene, but the reaction run time was significantly shorter, with complete conversion achieved within 90 min. Figure 6 illustrates one of the runs carried out with the

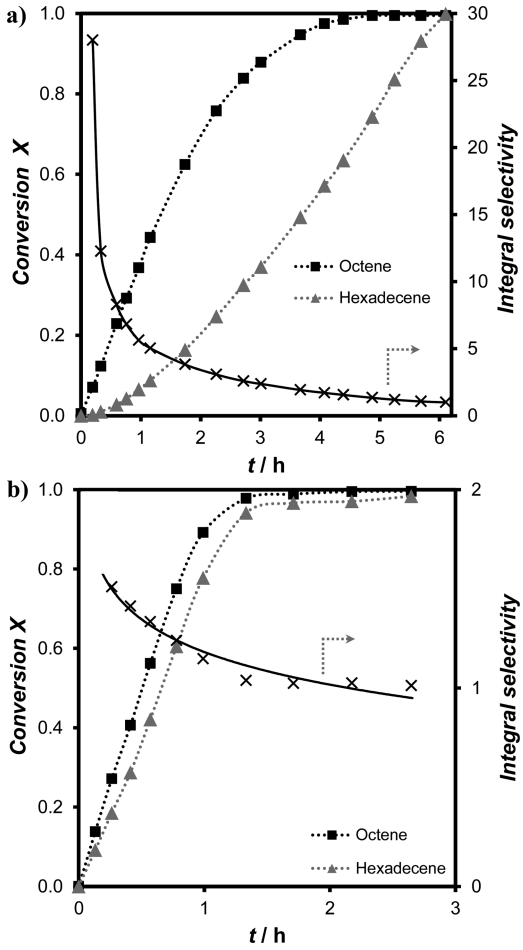

Figure 6. Conversion (primary *y*-axis) and the integral selectivity (conversion ratio octane/hexadecene, secondary *y*-axis) versus time profiles for the hydrogenation of a 1:1 mixture of 1-octene and 1-hexadecene over (a) Pt-MIL-101(Cr) catalyst and (b) platinum on alumina. Conditions: 91 mmol total olefin/mg Pt at reaction start, 1.5 bar hydrogen, 308 K.

1.2 wt % platinum loaded MOF composite catalyst. The conversion of octene and hexadecene is plotted along with the ratio of this conversion (integral selectivity). Clearly, at the reaction start, a high selectivity is shown for octane hydrogenation (at octene conversion of 7%, the octene/hexadecene selectivity ratio is 28). This preferential hydrogenation changes rapidly within the first 2 h of the reaction when more than 60% of octene is consumed. After this point, the consumption rate (slope of the plotted conversion) of hexadecene becomes comparable to that of octene as the reaction proceeds further. After 4 h, just over 97% of the octene is hydrogenated, and after ~6 h, the reaction is completed. Only after 4 h of reaction does the octene/hexadecene selectivity match that initially observed

dx.doi.org/10.1021/cs400681s | *ACS Catal.* 2013, 3, 2617−2626

for platinum on alumina: 1.5. For the octene/hexadecene hydrogenation, the reference catalyst *TOF* amounted to 21.0 s^{-1} (at ≈16 min, octene conversion was 27%), whereas that for the platinum-loaded MOF composite was 9.3 s^{-1} (at ≈20 min, octene conversion was 12%) (for the details of the reference catalyst, please refer to the Supporting Information; S3).

In the selective hydrogenation of pure benzonitrile, toluene and ammonia were not observed when using the MOF-based catalyst, but over Pt/alumina toluene, these were formed. Only benzylamine and dibenzylamine were observed for the MOF catalyst (Figure 7). At the start of the reaction, the integral

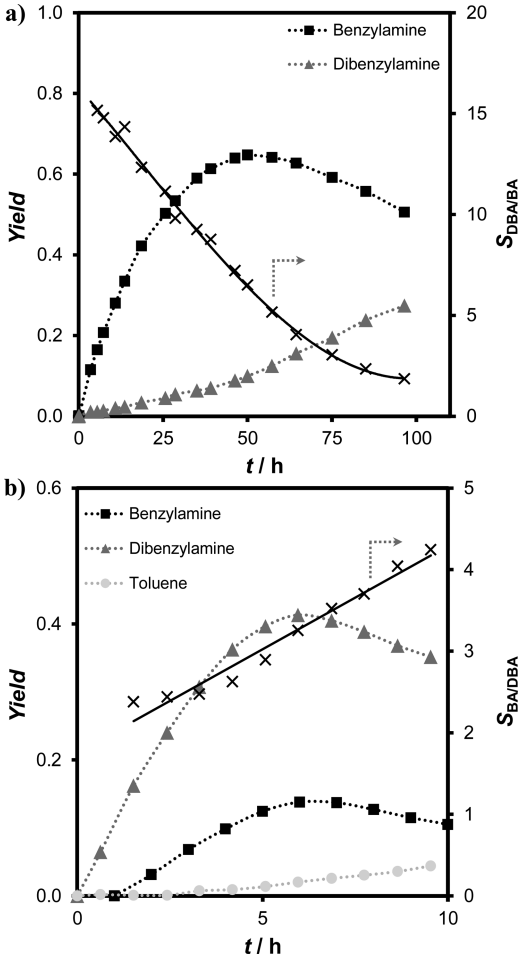

Figure 7. Yield (primary *y*-axis) and the integral selectivity (BA/DBA or DBA/BA ratio; secondary *y*-axis) versus time profiles for the solvent-free benzonitrile hydrogenation over (a) Pt-MIL-101(Cr) catalyst and (b) platinum on alumina. Conditions: 36.5 mmol benzonitrile/mg Pt at reaction start, 20 bar hydrogen, 308 K.

benzylamine/dibenzylamine selectivity is 15. This value declines steeply over the duration of 100 h that the reaction was allowed to proceed and comes to a value of 2. A maximum yield of 60% is achieved for benzylamine with a selectivity ratio of 6.5 at ∼50 h. In the literature, supported platinum has been extensively shown to be highly selective toward dibenzylamine.[52,56] This is confirmed for the reference Pt on alumina catalyst, in which dibenzylamine was the major component of the products, with a maximum integral DBA/BA selectivity of 4.2 at ∼9.5 h. Byproducts ammonia and toluene where detected in nearly all samples. It is striking that this selectivity is reversed in favor of benzylamine when hydrogenation occurs using Pt-MIL-101(Cr) catalyst (sample MIL-101(Cr) *Pt fully reduced*) (comparison made at 50% conversion of benzonitrile, 42% yield of benzylamine). The TOF of the platinum on alumina was calculated to be 0.8 s^{-1} at 92 min (from literature[53]), whereas the platinum-loaded MOF composite performed slightly worse, 0.5 s^{-1} (at 5.5 h).

In the hydrogenation of linoleic acid, cis/trans isomerization was not observed during the course of the reaction. The initial product ratio of oleic acid/stearic acid started initially at 12, but this decreased to 1.5 after 50 h (Figure 8). This oleic acid is

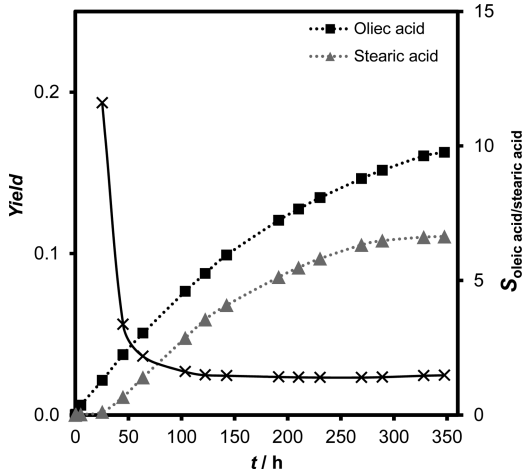

Figure 8. Yield (primary *y*-axis) and integral selectivity oleic/stearic acid (secondary *y*-axis) versus time profiles for the solvent-free linoleic acid hydrogenation over a Pt-MIL-101(Cr) catalyst. Conditions: 26 mmol linoleic acid/mg Pt at reaction start, 20 bar hydrogen, 308 K.

obtained directly after the reaction start, while stearic acid shows a sigmoidal profile, indicating being a consecutive reaction product. After 25 h, the production rate of stearic acid is in the same order of magnitude as that of oleic acid. When comparing results in Figure 8 with reference runs performed using platinum on alumina, there is no significant difference to distinguish the two catalysts. *TOF* numbers for the reference alumina and the MOF catalyst were found to be 1.5×10^{-4} s^{-1} (at 9 h, oleic acid had a yield of 9.1%) and 8.4×10^{-5} s^{-1} (taken at ≈25.5 h, oleic acid yield of 2.1%), respectively. For reference run profiles and repeated runs using Pt-MIL-101(Cr) catalyst, please refer to the Supporting Information; S4.

4. DISCUSSION

Platinum can be encapsulated in the MIL-101(Cr) metal organic framework with minimal localized damage to the support scaffold. The obtained Pt particles are slight bigger than the size of the cavities of the material,[82] inferring that some partial structure collapse takes place upon reduction and formation of the nanoparticles, as observed by the slight loss of crystallinity. However, this partial collapse does not seem to affect accessibility of the catalytic sites. Even after extensive usage, little loss of crytallinity is observed; the loss that is observed is caused mostly by attrition due to stirring in the reactor vessel. The resulting catalyst is active in the solvent-free hydrogenation of double bonds in alkenes and unsaturated fatty acids and of benzonitrile. Differences in selectivities have been observed in comparison with a Pt on alumina catalyst and, depending on the reactant, while the activity (*TOF*) is slightly lower. This is attributed to shape selectivity aspects and to the

dx.doi.org/10.1021/cs400681s | *ACS Catal.* 2013, 3, 2617−2626

structure of the MOF catalyst, as substantiated further below. It has been found that sonication is critical for achieving the reported desirable high Pt dispersion inside the MOF. Removing the sonication from this procedure produces dispersions comparable to that of purchased platinum on alumina catalyst. (For an overview of a sonication-free prepared MIL-101(Cr) catalyst, please refer to the Supporting Information; S5). The combination of an acidic treatment and growth of nanoparticles in the cages that exceed their size can result in local damage to the framework during the catalyst preparation. This alongside interference from the MOF's high surface area and the presence of poorly crystalline oxide Pt phases (so-called "XRD amorphous" Pt)[81−83] has resulted in the loss of XRD pattern quality when comparing pre- and postimpregnation results. On the basis of the absence of surface area loss, it can be inferred that the acidic treatment and nanoparticle growth did not have a significant effect on the overall integrity of the framework. With the comparison of XPS, ICP results, and the applied imaging techniques, the bulk distribution of Pt across the framework has been deduced. From the calculated Pt/Cr atomic ratios, we conclude that the vast majority of platinum in the MOF cages is close to the outer surface of the MIL-101 crystals, in an egg-shell configuration. Brønsted and Lewis acid sites have been identified in all MOF samples using in situ IR spectroscopy with CO as the probe molecule. It can be concluded that Lewis acidity associated with open Cr(III) sites decreases with the introduction of platinum nanoparticles, indicating that platinum is preferentially accommodated in close proximity to the chromium trimers.

The selectivity observed for the hydrogenation of selected α-olefins over platinum impregnated MIL-101(Cr) catalyst is attributed to the difference in chain length of substrate molecules and the relative molecular masses. Shape of substrate molecules does not and should not play any major role in the achieved results because the windows are sufficiently large to allow substrate molecules to enter the cages.[69−72,84] With the Wheeler−Weisz modulus >0.15 for the range of characteristic lengths for the produced catalyst, the criterion for negligible intraparticle mass transport effects in steady state is not fulfilled[85−87] so that the reaction is operated in the mass transport limiting regime is abundantly clear from the significantly longer duration that it takes for the MOF composite catalyst to complete the reaction compared with platinum on alumina (for the Wheeler−Weisz calculation, please refer to the Supporting Information; S6). The factor of 2 difference in the chain lengths of the olefins used determines faster transport of 1-octene to the active sites, and thus, a preferential selectivity for 1-octene is observed until this substrate is depleted. Such high selectivities have not been reported before under solvent-free conditions.[88−92]

The striking selectivity for benzylamine when hydrogenating using Pt-MIL-101(Cr) catalyst can be interpreted when considering the limited space (steric hindrance) caused by the deposition of Pt nanoparticles in the cages. The result is the blocking of the reaction pathway by steric constraints, which has resulted in dibenzylamine being marginally formed. A small fraction of Pt nanoparticles at the outer surface of the catalyst, as observed in SEI-components images, is primarily responsible for the formation of dibenzylamine. When comparing results to what has been previously reported for platinum based catalysts, it becomes apparent that this selectivity has been turned around. Conventionally, platinum favors dibenzylamine over benzylamine,[53,55−57] which has been extensively shown for various supports.

The evolution of observed products for the hydrogenation of linoleic acid shows the similar behavior of the Pt-MIL-101(Cr) and the reference catalyst, although at a much lower rate. The similar product scope is attributed to the small differences in size between the possible reaction products. These results are in line with other catalysts, such as palladium on carbon, for which products of double bond migration are also observed.[85] Under the pressures considered here, these byproducts are not observed, but the oleic and stearic acid profiles are undoubtedly the same for both catalysts. Solvent-free hydrogenation of linoleic acid is strongly limited by the accessibility of the platinum, which in this case is exclusively the Pt located on the outer surface of the catalyst. Platinum on alumina is better accessible and, thus, results in the observed higher rate.

For all reactions, the observed selectivities were found to be independent of the number of runs a batch of catalyst had been used. This is despite a small loss in the turnovers, clearly observed in the case of the α-olefin mixture and benzonitrile hydrogenation. Even in combination with the loss of surface area and slight loss of crystallinity, no significant change in the relevant selectivities has been observed. It is thus justified that the accessibility to the active sites in the catalyst has not been altered during the course of catalytic testing.

5. CONCLUSIONS

Highly dispersed platinum nanoparticles have been successfully incorporated into the MIL-101(Cr) framework using wet impregnation in combination with a two-stage reduction step. It has been shown that platinum catalysts with a loading of 1.2 wt % and an average particle size of 4.3 nm according to CO chemisorption can be easily prepared. These particles are larger than cages of MIL-101. It has been deduced that the platinum nanoparticles reside inside of the pores of the framework and are in close proximity to the chromium trimers found in MIL-101(Cr) and close to the particle surface in an egg-shell configuration. The oxidation state of platinum was determined using XPS, which showed the presence of a minute amount of PtCl as well as PtO that had formed from the reduced Pt^0.

The selective hydrogenation of an olefin mixture of 1-octene and 1-hexadecene demonstrated mass transport limitations, giving rise to enhanced selectivities. This selectivity was observed prior to 1-octene depletion and is attributed to the differences in the chain lengths of substrate molecules that results in mass transport limitations in the MOF pores. In the hydrogenation of benzonitrile, selectivity of supported platinum nanoparticles toward dibenzylamine was flipped toward benzylamine by placing the active sites inside the MOF pores structure. This sudden change in selectivity has been attributed to transition state selectivity. The selective hydrogenation of linoleic acid was also investigated; however, higher selectivities could not be achieved by the platinum MOF catalyst when compared with platinum on alumina.

■ ASSOCIATED CONTENT

Supporting Information

Additional information as noted in the text. This material is available free of charge via the Internet at http://pubs.acs.org.

dx.doi.org/10.1021/cs400681s | ACS Catal. 2013, 3, 2617−2626

AUTHOR INFORMATION

Corresponding Author

*Phone.+31 (0)15 278 9820. Fax.+31 (0)15 278 5006. E-mail: H.Khajavi@tudelft.nl, J.Gascon@tudelft.nl.

Notes

The authors declare no competing financial interest.

ACKNOWLEDGMENTS

The authors thank Shell for hosting this research at Shell Technology Centre Amsterdam, and Shell Researcher Sipke Wadman for fruitful discussions and his support.

REFERENCES

(1) Chui, S. S.; Lo, S. M.; Charmant, J. P.; Orpen, A. G.; Williams, I. D. *Science* **1999**, *283*, 1148−1150.
(2) Schüth, F.; Schmidt, W. *Adv. Mater.* **2002**, *14*, 629−638.
(3) Nuzhdin, A. L.; Dybtsev, D. N.; Bryliakov, K. P.; Talsi, E. P.; Fedin, V. P. *J. Am. Chem. Soc.* **2007**, *129*, 12958−12959.
(4) Alkordi, M. H.; Liu, Y.; Larsen, R. W.; Eubank, J. F.; Eddaoudi, M. *J. Am. Chem. Soc.* **2008**, *130*, 12639−12641.
(5) Farha, O. K.; Mulfort, K. L.; Hupp, J. T. *Inorg. Chem.* **2008**, *47*, 10223−10225.
(6) Lee, J.; Farha, O. K.; Roberts, J.; Scheidt, K. A.; Nguyen, S. T.; Hupp, J. T. *Chem. Soc. Rev.* **2009**, *38*, 1450−1459.
(7) Dhakshinamoorthya, A.; Garcia, H. *Chem. Soc. Rev.* **2012**, *41*, 5262−5284.
(8) Wu, C. D.; Hu, A.; Zhang, L.; Lin, W. *J. Am. Chem. Soc.* **2005**, *127*, 8940−8941.
(9) Lu, G.; Li, S.; Guo, C.; Farha, O. K.; Hauser, B. G.; Qi, X.; Wang, Y.; Wang, X.; Han, S.; Liu, X.; DuChene, J. S.; Zhang, H.; Zhang, Q.; Chen, X.; Ma, J.; Loo, S. C. J.; Wei, W. D.; Yang, Y.; Hupp, J. T.; Huo, F. *Nat. Chem.* **2012**, *4*, 310−316.
(10) Horike, S.; Dinca, M.; Tamaki, K.; Long, J. R. *J. Am. Chem. Soc.* **2008**, *130*, 5854−5855.
(11) Corma, A.; García, H.; Llabrés i Xamena, F. *Chem. Rev.* **2010**, *110*, 4606−4655.
(12) Adamsa, R.; Carsona, C.; Warda, J.; Tannenbaumb, R.; Koros, W. *Microporous Mesoporous Mater.* **2010**, *131*, 13−20.
(13) Gücüzyener, C.; van den Bergh, J.; Gascon, J.; Kapteijn, F. *J. Am. Chem. Soc.* **2010**, *50*, 17704−17706.
(14) Pan, Y.; Lai, Z. *Chem. Commun.* **2011**, *47*, 10275−10277.
(15) Remi, J. C. S.; Rémy, T.; Van Hunskerken, V.; van de Perre, S.; Duerinck, T.; Maes, M.; De Vos, D.; Gobechiya, E.; Kirschhock, C. E. A.; Baron, G. V.; Denayer, J. F. M. *ChemSusChem.* **2011**, *4*, 1074−1077.
(16) van den Bergh, J.; Gucuyener, C.; Pidko, E. A.; Hensen, E. J. M.; Gascon, J.; Kapteijn, F. *Chem.—Eur. J.* **2011**, *17*, 8832−8840.
(17) Zou, X.; Zhang, F.; Thomas, S.; Zhu, G.; Valtchev, V.; Mintova, S. *Chem.—Eur. J.* **2011**, *17*, 12076−12083.
(18) Llabrés i Xamena, F. X.; Corma, A.; Garcia, H. *J. Phys. Chem., C* **2007**, *111*, 80−85.
(19) Alvaro, M.; Carbonell, E.; Ferrer, B.; Llabrés i Xamena, F. X.; Garcia, H. *Chem.—Eur. J.* **2007**, *13*, 5106−5112.
(20) *International Roadmap for Semiconductors*; Semiconductor Industry Association: Washington, DC, 2007.
(21) Srivastava, S.; Kotov, N. A. *Soft Matter* **2009**, *5*, 1146−1156.
(22) Zhang, W. X.; Yang, S. H. *Acc. Chem. Res.* **2009**, *42*, 1617−1627.
(23) Toksoz, S.; Acar, H.; Guler, M. O. *Soft Matter* **2010**, *6*, 5839−5849.
(24) Allendorf, M. D.; Schwartzberg, A.; Stavila, V.; Talin, A. A. *Chem.—Eur. J.* **2011**, *17*, 11372−11388.
(25) Khajavi, H.; Gascon, J.; Schins, J. M.; Siebbeles, L. D. A.; Kapteijn, F. *J. Phys. Chem. C* **2011**, *115*, 12487−12493.
(26) Wang, M.; Guo, S.; Li, Y.; Cai, L.; Zou, J.; Xu, G.; Zhou, W.; Zheng, F.; Guo, G. *J. Am. Chem. Soc.* **2009**, *131*, 13572−13573.
(27) Harbuzaru, B. V.; Corma, A.; Rey, F.; Jordá, J. L.; Ananias, D.; Carlos, L. D.; Rocha. *J. Angew. Chem. Int. Ed.* **2009**, *48*, 6476−6479.
(28) Wang, M.; Guo, S.; Li, Y.; Cai, L. J.; Zou, G.; Xu, W.; Zhou, F.; Zheng, G.; Guo. *J. Am. Chem. Soc.* **2009**, *131*, 13572−13573.
(29) Silva, C. G.; Luz, I.; i Xamena, F. X. L. A.; Corma, H.; García. *Chem.—Eur. J.* **2010**, *16*, 11133−11138.
(30) Choi, J. R.; Tachikawa, T.; Fujitsuka, M.; Majima, T. *Langmuir* **2010**, *26*, 10437−10443.
(31) Liu, Y.; Pan, M.; Yang, Q.; Fu, L.; Li, K.; Wei, S.; Su, C. *Chem. Mater.* **2012**, *24*, 1954−1960.
(32) Horcajada, P.; Serre, C.; Maurin, G.; Ramsahye, N. A.; Balas, F.; Vallet-Regí, M.; Sebban, M.; Taulelle, F.; Férey, G. *J. Am. Chem. Soc.* **2008**, *130*, 6774−6780.
(33) Huxford, R. C.; Rocca, J. D.; Lincorresponding, W. *Curr. Opin. Chem. Biol.* **2010**, *14*, 262−268.
(34) Keskin, S.; Kızılel, S. *Ind. Eng. Chem. Res.* **2011**, *50*, 1799−1812.
(35) Long, J. R.; Yaghi, O. M. *Chem. Soc. Rev.* **2009**, *38*, 1213−1214.
(36) Vermoortele, F.; Ameloot, R.; Alaerts, L.; Matthessen, R.; Carlier, B.; Ramos-Fernandez, E. V.; Gascon, J.; Kapteijn, F.; De Vos, D. E. *J. Mater. Chem.* **2012**, *22*, 10313−10321.
(37) Goesten, M. G.; Alcañiz, J. J.; Ramos-Fernandez, E. V.; Sai Sankar Gupta, K. B.; Stavitski, E.; van Bekkum, H.; Gascon, J.; Kapteijn, F. *J. Catal.* **2011**, *281*, 177−187.
(38) Cirujano, F. G.; Leyva-Pérez, A.; Corma, A.; Llabrés i Xamena, F. *Chem. Cat. Chem.* **2013**, *5*, 538−549.
(39) Li, H.; Zhu, Z.; Zhang, F.; Xie, S.; Li, H.; Li, P.; Zhou, X. *ACS Catal.* **2011**, *1*, 1604−1612.
(40) Juan-Alcañiz, J.; Gascon, J.; Kapteijn, F. *J. Mater. Chem.* **2012**, *22*, 10102−10118.
(41) Pan, Y.; Yuan, B.; Li, Y.; He, D. *Chem. Commun.* **2010**, *46*, 2280−2282.
(42) Yuan, B.; Pan, Y.; Li, Y.; Yin, B.; Jiang, H. *Angew. Chem., Int. Ed.* **2010**, *49*, 4054−4058.
(43) Shultz, A. M.; Farha, O. K.; Hupp, J. T.; Nguyen, S. T. *J. Am. Chem. Soc.* **2009**, *131*, 4204−4205.
(44) Ramos-Fernandez, E. V.; Pieters, C.; van der Linden, B.; Juan-Alcañiz, J.; Serra-Crespo, P.; Verhoeven, M. W. G. M.; Niemantsverdriet, H. J.; Gascon, F.; Kapteijn. *J. Catal.* **2012**, *289*, 42−52.
(45) Meilikhov, M.; Yusenko, K.; Esken, D.; Turner, S.; Van Tendeloo, G.; Fischer, R. A. *Eur. J. Inorg. Chem.* **2010**, 3701−3714.
(46) Aijaz, A.; Karkamkar, A.; Joon Choi, Y.; Tsumori, N.; Rönnebro, E.; Autrey, T.; Shioyama, H.; Xu, Q. *J. Am. Chem. Soc.* **2012**, *134*, 13926−13929.
(47) Cirujano, F. G.; Leyva-Pérez, A.; Corma, A.; Llabrés i Xamena, F. X. *ChemCatChem* **2013**, *5*, 538−549.
(48) Shirley, D. A. *Phys. Rev. B* **1972**, *12*, 4709−4714.
(49) Nishimura, S. *Handbook of Heterogeneous Catalytic Hydrogenation for Organic Synthesis*; Wiley-VCH: New York, 2001, pp 254−285.
(50) De Bellefon, C.; Fouilloux, P. *Catal. Rev. Sci. Eng.* **1994**, *36*, 459−506.
(51) *Catalytic Hydrogenation*; Volf, J., Pasek, J., Cerveny, L., Eds.; Elsevier, Amsterdam, 1986, 105−106.
(52) Gomez, S.; Peters, J. A.; Maschmeyer, T. *Adv. Synth. Catal.* **2002**, *344*, 1037−1057.
(53) Bakker, J. J. W.; van der Neut, A. G.; Kreutzer, M. T.; Moulijn, J. A.; Kapteijn, F. *J. Catal.* **2010**, *274*, 176−191.
(54) Sabatier, P.; Senderens, J. R.; Hebd, C. R. *Seances Acad. Sci.* **1905**, *140*, 482.
(55) Mignonac, G.; Hebd, C. R. *Seances Acad. Sci.* **1920**, *171*, 114−117.
(56) von Braun, J.; Blessing, G.; Zobel, F. *Chem. Ber.* **1923**, *36*, 1988−2001.
(57) Kindler, K.; Hesse, F. *Arch. Pharm.* **1933**, *27*, 439−445.
(58) Greenfield, H. *Ind. Eng. Chem. Prod. Res. Dev.* **1976**, *15*, 156−158.
(59) Huang, Y.; Sachtler, W. M. H. *J. Catal.* **1999**, *184*, 247−261.
(60) Bernas, A.; Kumar, N.; Mäki-Arvela, P.; Kul'kova, N. V.; Holmbom, B.; Salmi, T.; Murzin, D. Yu. *Appl. Catal., A* **2003**, *245*, 257−275.

(61) Kitayama, Y.; Muraoka, M.; Takahashi, M.; Kodama, T.; Takahashi, E.; Okamura, M. *J. Am. Oil Chem. Soc.* **1997**, *74*, 525−529.
(62) Bernas, A.; Myllyoja, J.; Salmi, T.; Murzin, D. Yu. *Appl. Catal., A* **2009**, *353*, 166−180.
(63) Sim, K. S.; Hilaire, L.; Le Normand, F.; Touroude, R.; Paul-Boncour, V.; Percheron-Guegan, A. *J. Chem. Soc., Faraday Trans.* **1991**, *87*, 1453.
(64) Rylander, P. *Organic Synthesis with Noble Metal Catalysts*; Academic Press: New York, 1979, pp 36−37.
(65) Bernas, A.; Laukkanen, P.; Kumar, N.; Mäki-Arvela, P.; Väyrynen, J.; Laine, E.; Holmbom, B.; Salmi, T.; Murzin, D. Yu. *J. Catal.* **2002**, *210*, 354−366.
(66) Bernas, A.; Kumar, N.; Mäki-Arvela, P.; Laine, E.; Holmbom, B.; Salmi, T.; Murzin, D. Yu. *Chem. Commun.* **2002**, *10*, 1142−1143.
(67) Cheah, K. Y.; Tang, T. S.; Mizukami, F.; Niwa, S.; Toba, M.; Choo, Y. M. *J. Am. Oil Chem. Soc.* **1992**, *69*, 410−416.
(68) Ramos-Fernandez, E. V.; Garcia-Domingos, M.; Juan-Alcañiz, J.; Gascon, J.; Kapteijn, F. *Appl. Catal., A* **2011**, *391*, 261−267.
(69) Férey, G.; Mellot-Draznieks, C.; Serre, C.; Millange, F.; Dutour, J.; Surblé, S.; Margiolaki, I. *Science* **2005**, *309*, 2040−2042.
(70) Sonnauer, A.; Hoffmann, F.; Fröba, M.; Kienle, L.; Duppel, V.; Thommes, M.; Serre, C.; Férey, G.; Stock, N. *Angew. Chem., Int. Ed.* **2009**, *121*, 3849−3852.
(71) Bromberg, L.; Diao, Y.; Wu, H.; Speakman, S. A.; Hatton, T. A. *Chem. Mater.* **2012**, *24*, 1664−1675.
(72) Hadjiivanov, K.; Vayssilov, G. *Adv. Catal.* **2002**, *47*, 307−511.
(73) Kubanek, P.; Schmidt, H. W.; Spliethoff, B.; Schuth, F. *Microporous Mesoporous Mater.* **2005**, *77*, 89−96.
(74) Chakarova, K.; Mihaylov, M.; Hadjiivanov, K. *Microporous Mesoporous Mater.* **2005**, *81*, 305−312.
(75) Bazin, P.; Saur, O.; Lavalley, J. C.; Daturi, M.; Blanchard, G. *Phys. Chem. Chem. Phys.* **2005**, *7*, 187−194.
(76) Vimont, A.; Goupil, J. M.; Lavalley, J. C.; Daturi, M.; Surblé, S.; Serre, C.; Millange, F.; Férey, G.; Audebrand, N. *J. Am. Chem. Soc.* **2006**, *128*, 3218−3227.
(77) Morrow, B. A.; Ramamurt, P. *Can. J. Chem.* **1971**, *49*, 3409−3410.
(78) Vimont, A.; Thibault-Starzyk, F.; Daturi, M. *Chem. Soc. Rev.* **2010**, *39*, 4928−4950.
(79) Amorim, C.; Keane, M. A. *J. Colloid Interface Sci.* **2008**, *322*, 196−208.
(80) Fagherazzi, G.; Benedetti, A.; Polizzi, S.; Mario, A.; Pinna, F.; Signoretto, M.; Pernicone, N. *Catal. Lett.* **1995**, *32*, 293−303.
(81) Sa, J.; Arteaga, G. D.; Daley, R. A.; Bernardi, J.; Anderson, J. A. *J. Phys. Chem. B* **2006**, *110*, 17090−17095.
(82) Aijaz, A.; Karkamkar, A.; Choi, Y. J.; Tsumori, N.; Rönnebro, E.; Autrey, T.; Shioyama, H.; Xu, Q. *J. Am. Chem. Soc.* **2012**, *34*, 13926−13929.
(83) Hyde, T. *Platinum Met. Rev.* **2008**, *52*, 129−130.
(84) Henschel, A.; Senkovska, I.; Kaskel, S. *Adsorption* **2011**, *17*, 219−226.
(85) Bernas, A.; Myllyoja, J.; Salmi, T.; Murzin, D. Yu. *Appl. Catal., A* **2009**, *353*, 166−180.
(86) Weisz, P. B.; Prater, C. D. *Adv. Catal.* **1954**, *6*, 143−148.
(87) Dekker, F. H. M.; Bliek, A.; Kapteijn, F.; Moulijn, J. A. *Chem. Eng. Sci.* **1995**, *22*, 3573−3580.
(88) Červený, L.; Růžićka, V. *Catal. Rev.: Sci. Eng.* **1982**, *24*, 503−566.
(89) Červený, L.; Růžićka, V. *Adv. Catal.* **1981**, *30*, 335−338.
(90) Červený, L.; Růžićka, V. *Sb. Vys. Sk. Chem. Technol. Praze* **1973**, *5*, C19.
(91) Růžićka, V.; Červený, L. *J. Prakt. Chem.* **1969**, *135*, 311−315.
(92) Červený, L.; Červená, J.; Růžićka, V. *Collect. Czech. Chem. Commun.* **1972**, *37*, 2946−2953.